Modeling of Casting, Welding and Advanced Solidification Processes - XI
Edited by Charles-André Gandin and Michel Bellet
TMS (The Minerals, Metals & Materials Society), 2006

PHASE FIELD THEORY OF POLYCRYSTALLINE FREEZING IN THREE DIMENSIONS

Tamás Pusztai, Gábor Bortel, László Gránásy
Research Institute for Solid State Physics and Optics; H-1525 Budapest, POB 49, Hungary

Keywords: Phase field theory, three dimensions, thin films, polycrystals, dendrites

Abstract

A phase field theory, we proposed recently to describe nucleation and growth in three dimensions (3D), has been used to study the formation of polycrystalline patterns in the alloy systems Al-Ti and Cu-Ni. In our model, the free energy of grain boundaries is assumed proportional to the angular difference between the adjacent crystals expressed in terms of the differences of the four symmetric Euler parameters called quaternions. The equations of motion for these fields have been obtained from variational principles. In the simulations cubic crystal symmetries are considered. We investigate the evolution of polydendritic morphology, present simulated analogies of the metallographic images, and explore the possibility of modeling solidification in thin layers. Transformation kinetics in the bulk and in thin films is discussed in terms of the Johnson-Mehl-Avrami-Kolmogorov approach.

Introduction

The physical properties of bulk polycrystalline materials produced by far-from-equilibrium freezing depend on the size, shape and composition distributions of the crystal grains they contain [1]. Despite extensive research done in the past decades, many details of polycrystalline solidification are poorly understood, such as the kinetics of anisotropically growing randomly oriented particles (e.g., dendrites and polycrystalline aggregates). Crystallization of thin films, whose thickness falls in the range of a few tens of nanometers to a few microns, is also of scientific and practical importance [2-5]. Recent studies indicate that the layer thickness may influence growth morphology [4,5]. Three dimensional simulations of polycrystalline solidification are expected to contribute to a better understanding of the relevant processes.

Recently, the phase field theory became a method of choice when modeling complex solidification patterns [6]. While various aspects of polycrystalline solidification have been addressed previously within the phase field theory [7], description of systems with anisotropic growth needs further attention. The main difficulty here is that for describing an anisotropic growth of individual particles one needs to consider the crystallographic orientation of all grains. While in the multi-phase field models [8,9] handling of this problem and the mimicking of nucleation via inserting supercritical crystallites into the simulation window "by hand" are straightforward, the possibility for a Langevin-type physical modeling of crystal nucleation is less obvious.

Building on previous work by Kobayashi et al. [10], we recently developed a phase field theory that successfully addressed the noise-induced nucleation of crystallites with different crystallographic orientation in two-dimensional (2D) systems [11]. Our approach describes the formation of such complex polycrystalline growth patterns as dendrites disordered by foreign particles [12], fractallike aggregates, and spherulites [13]. Until recently, simulation of complex polycrystalline growth patterns has been restricted to two dimensions. While in 2D a single field is sufficient to describe the local crystallographic orientation, relative to which the anisotropies of the interfacial

and dynamic properties are counted, in 3D at least three parameter fields (e.g., the Euler angles) are needed to formulate the theory. We have recently developed a 3D model of polycrystalline solidification (nucleation and growth) [14]. At essentially the same time, a similar approach has been independently developed by Kobayashi and Warren for describing grain coarsening in 3D polycrystals [15].

Herein, we use our 3D model of polycrystalline solidification [14] to address morphology evolution and transformation kinetics during crystallization in bulk regions and thin films.

Phase Field Theory of Polycrystalline Solidification in 3D

A free energy functional that consists of the usual square-gradient, double well and driving force terms is used, a model equivalent to the entropy formulation by Warren and Boettinger [16].

$$F = \int d^3 r \left\{ \frac{\varepsilon_\phi^2 T}{2} |\nabla \phi|^2 + f(\phi, c, T) \right\}, \tag{1}$$

where the local phase state of matter (solid or liquid) is characterized by the phase field ϕ (a structural order parameter) and the solute concentration c, ε_ϕ is a constant, T is the temperature. The gradient term for the phase field leads to a diffuse crystal-liquid interface, a feature observed both in experiment and computer simulations. The local free energy density is assumed to have the form $f(\phi, c, T) = w(\phi)T\, g(\phi) + [1 - p(\phi)]\, f_S(c) + p(\phi)\, f_L(c)$, where the "double well" and "interpolation" functions have the forms $g(\phi) = {}^1/_4\, \phi^2(1-\phi)^2$ and $p(\phi) = \phi^3(10 - 15\phi + 6\phi^2)$, respectively, while the free energy scale is $w(\phi) = (1 - c)\, w_A + c\, w_B$ [16]. The respective free energy surface has two minima ($\phi = 0$ and $\phi = 1$, corresponding to the crystalline and liquid phases), whose relative depth is the driving force for crystallization and is a function of both temperature and composition as specified by the free energy densities in the bulk solid and liquid, $f_{S,L}(c,T)$, taken here from the ideal solution model.

Time evolution is described by the following equations of motion:

$$\dot{\phi} = -M_\phi \frac{\delta F}{\delta \phi} + \zeta_\phi = M_\phi \left\{ \nabla \left(\frac{\partial I}{\partial \nabla \phi} \right) - \frac{\partial I}{\partial \phi} \right\} + \zeta_\phi, \tag{2}$$

$$\dot{c} = \nabla M_c \nabla \left(\frac{\delta F}{\delta c} - \zeta_j \right) = \nabla \left\{ \frac{v_m}{RT} Dc(1-c) \nabla \left[\frac{\partial I}{\partial \phi} - \nabla \left(\frac{\partial I}{\partial \nabla \phi} \right) - \zeta_j \right] \right\}, \tag{3}$$

where I is the total free energy density (including the gradient terms), v_m is the molar volume, D the diffusion coefficient in the liquid, and ζ_i are the appropriate noise terms. The time scales for the two fields are determined by the mobility coefficients appearing in the coarse-grained equations of motion: M_ϕ and M_c. These coarse-grained mobilities can be taken from experiments and/or evaluated from atomistic simulations [6]. For example, the mobility M_c, is directly proportional to the classic inter-diffusion coefficient for a binary mixture, the mobility M_ϕ dictates the rate of crystallization. We solve these equations numerically in three dimensions with an anisotropic interface free energy, $\gamma = \gamma_0 \{1 - 3\varepsilon_{3D} + 4\varepsilon_{3D} [(\nabla\phi)_x^4 + (\nabla\phi)_y^4 + (\nabla\phi)_z^4] / |\nabla\phi|^4\}$.

The *local crystallographic* orientation is considered as the relative orientation of a local coordinate system (fixed to the crystal lattice) with respect to a reference system (fixed to the laboratory frame). In 3D, the relative orientation with respect to the laboratory system is uniquely defined by a single rotation of angle η around a specific axis $\boldsymbol{c}$, and can be expressed in terms of

the three Euler angles. However, this representation has disadvantages: It has divergences at the poles $\vartheta = 0$ and π, and one has to use trigonometric functions that are time consuming in numerical calculations. Therefore, we opt for the four symmetric Euler parameters, $q_0 = \cos(\eta/2)$, $q_1 = c_1 \sin(\eta/2)$, $q_2 = c_2 \sin(\eta/2)$, and $q_3 = c_3 \sin(\eta/2)$, a representation free of such difficulties. (Here c_i are the components of the unit vector $\boldsymbol{c}$ of the rotation axis.) These four parameters $\boldsymbol{q} = (q_0, q_1, q_2, q_3)$, often referred to as *quaternions*, satisfy the relationship $\sum_i q_i^2 = 1$, therefore, can be viewed as a point on the four-dimensional (4D) unit sphere [17]. (Here $\sum_i$ stands for summation with respect to $i = 0$, 1, 2, and 3, a notation used throughout this paper.)

The angular difference δ between two orientations represented by quaternions $\boldsymbol{q_1}$ and $\boldsymbol{q_2}$ can be expressed as $\cos(\delta) = \frac{1}{2}[\mathrm{Tr}(\mathbf{R}) - 1]$, where the matrix of rotation $\mathbf{R}$ is related to the individual rotation matrices $\mathbf{R}(\boldsymbol{q_1})$ and $\mathbf{R}(\boldsymbol{q_2})$, that rotate the reference system into the corresponding local orientations, as $\mathbf{R} = \mathbf{R}(\boldsymbol{q_1})\cdot\mathbf{R}(\boldsymbol{q_2})^{-1}$. After lengthy but straightforward algebraic manipulations one finds that the angular difference can be expressed in terms of the differences of quaternion coordinates: $\cos(\delta) = 1 - 2\Delta^2 + \Delta^4/2$, where $\Delta^2 = (\boldsymbol{q}_2 - \boldsymbol{q}_1)^2 = \sum_i \Delta q_i^2$, is the square of the Euclidian distance between the points $\boldsymbol{q_1}$ and $\boldsymbol{q_2}$ on the 4D unit sphere. Comparing this expression with the Taylor expansion of the function $\cos(\delta)$, one finds that 2Δ is indeed an excellent approximation of δ. Relying on this approximation, we express the orientational difference as $\delta \approx 2\Delta$.

The free energy of small-angle grain boundaries increases approximately linearly with the misorientation of the neighboring crystals, saturating at about twice of the free energy of the solid-liquid interface. Our goal is to reproduce this behavior of the small angle grain boundaries. To penalize spatial changes in the crystal orientation, in particular the presence of grain boundaries, we introduce an orientational contribution f_{ori} to the integrand of the free energy functional, which is invariant to rotations of the whole system. In 3D, we postulate [14]

$$f_{ori} = 2HT[1 - p(\phi)]\left\{\sum_i (\nabla q_i)^2\right\}^{1/2}, \tag{4}$$

a definition that boils down to the 2D model, provided that the orientational transition across the grain boundary has a fixed rotation axis as in 2D.

To model crystal nucleation in the liquid, the orientation fields $\boldsymbol{q}(\mathbf{r})$ are extended to the liquid, where they are made to fluctuate in time and space [14]. Assigning local crystal orientation to liquid regions, even a fluctuating one, may seem artificial at first sight. However, due to geometrical and/or chemical constraints, a short-range order exists even in simple liquids, which is often similar to the one in the solid. Rotating the crystalline first-neighbor shell so that it aligns optimally with the local liquid structure, one may assign a local orientation to every atom in the liquid. The orientation obtained in this manner fluctuates in time and space. The correlation of the atomic positions/angles shows how good this fit is. (In the model, the fluctuating orientation fields and the phase field play these roles.) Approaching the solid from the liquid, the orientation becomes more definite (the amplitude of the orientational fluctuations decreases) and matches to that of the solid, while the correlation between the local liquid structure and the crystal structure improves. f_{ori} recovers this behavior by realizing a strong coupling between the orientation and phase fields.

Note that f_{ori} consists of the factor $(1 - p(\phi))$ to avoid double counting the orientational contribution in the liquid, which is *per definitionem* incorporated into the free energy of the bulk liquid. With appropriate choice of the model parameters, an ordered liquid layer surrounds the crystal as seen in atomistic simulations.

Time evolution of the orientation fields is governed by relaxational dynamics both in 2D and 3D, and noise terms are added to model the thermal fluctuations. In deriving the equations of motion for the quaternion fields, we need to take into account the quaternion properties ($\sum_i q_i^2 = 1$), which is done using the method of Lagrange multipliers,

$$\frac{\partial q_i}{\partial t} = -M_q \frac{\delta F}{\delta q_i} + \zeta_i = M_q \left\{ \nabla \left(\frac{\partial I}{\partial \nabla q_i} \right) - \frac{\partial I}{\partial q_i} \right\} + \zeta_i \,, \tag{5}$$

where M_q is the common mobility coefficient for the symmetric quaternion fields, I is the total free energy density (including the gradient terms and the term with the Lagrange multiplier), while ζ_i are the appropriate noise terms [14]. Utilizing the relationship $\sum_i q_i \, (\partial q_i/\partial t) = 0$ that follows from the quaternion properties, and expressing the Lagrange multiplier in terms of q_i and ∇q_i, the equation of motion for the orientation (quaternion) fields can be expressed as [14]

$$\frac{\partial q_i}{\partial t} = M_q \left\{ \nabla \left(HT[1-p(\phi)] \frac{\nabla q_i}{\left[\sum_l (\nabla q_l)^2 \right]^{1/2}} \right) - q_i \sum_k q_k \nabla \left(HT[1-p(\phi)] \frac{\nabla q_k}{\left[\sum_l (\nabla q_l)^2 \right]^{1/2}} \right) \right\} + \zeta_i \,. \tag{6}$$

Gaussian white noises of amplitude $\zeta_i = \zeta_{S,i} + (\zeta_{L,i} - \zeta_{S,i})\, p(\phi)$ have been added to the orientation fields so that the quaternion properties of the q_i fields are retained. ($\zeta_{L,i}$ and $\zeta_{S,i}$ are the amplitudes in the liquid and solid.)

This formulation of the model is valid for triclinic lattice without symmetries (space group P1). In the case of other crystals, the crystal symmetries yield equivalent orientations that do not form grain boundaries. These symmetries can be taken into account, when discretizing the differential operators used in the equations of motions for the quaternion fields. Calculating the angular difference between a cell and its neighbors, all equivalent orientations of the neighbor have to be considered. The respective angular differences δ are calculated (using matrices of rotation $\mathbf{R'} = \mathbf{R}\cdot\mathbf{S}\cdot\mathbf{R}^{-1}$, where $\mathbf{S}$ is a symmetry operator), of which the smallest δ value shall be used in calculating the differential operator.

Numerical Solution

The equations of motion have been solved numerically using an explicit finite difference scheme. In modeling crystallization in the bulk, periodic boundary conditions are used. In contrast, reduced thickness, and "no-flux" boundary conditions have been applied in the calculations for thin films. The latter corresponds to a chemically inert glassy container of a 90° contact angle at the wall-crystal-liquid triple junction. The time and spatial steps were chosen to ensure stability of our solutions. The noise has been discretized as described by Karma and Rappel [18]. A parallel code has been developed and run on two PC clusters, consisting of 60 and 100 nodes, respectively.

Physical Properties

In the present computations, we use the physical properties of the Cu-Ni [16] and Al-Ti system of technological interest [19]. In the Cu-Ni system, the calculations were performed at 1574 K and at a supersaturation of $S = (c_L - c)/(c_L - c_S) = 0.75$, where $c_L = 0.466219$, $c_S = 0.399112$ and c are the concentrations at the liquidus, solidus, and the initial homogeneous liquid mixture, respectively. The diffusion coefficient in the liquid was assumed to be $D_L = 10^{-9}$ m^2/s. Dimensionless mobilities of $M_{\phi,0L} = 3.55\times10^{-1}$ m^3/Js and $M_{q,L} = 8.17$ m^3/Js, and $M_{q,S} = 0$ were applied,

while $D_S = 0$ was taken in the solid. In the Al-Ti system, partial solidification of the $Al_{50.8}Ti_{49.2}$ composition (formation of β-Ti + interdendritic liquid) has been studied at 1723 K. Thermodynamic properties were communicated to us by Dinsdale [20]. Other properties were taken from [21]. Dendritic growth in the present simulations originates from the anisotropy of either the phase field mobility $M_\phi = M_{\phi,0}\{1 - 3\varepsilon_{3D} + 4\varepsilon_{3D}\,[(\nabla\phi)_x^4 + (\nabla\phi)_y^4 + (\nabla\phi)_z^4]/|\nabla\phi|^4\}$ that reflects the orientation dependence of the molecular attachment kinetics [6] or of the interfacial free energy assumed to have a similar functional form (see above). Since the physical thickness of the interface is in the nanometer range and the typical solidification structures are far larger (μm to mm), a full simulation of polycrystalline solidification from nucleation to particle impingement cannot be performed even with the fastest of the present supercomputers. Since we seek here a qualitative understanding, following previous work [10-14,16], the interface thickness has been increased $d = 20.6$ nm, while the interface free energy of the pure constituents has been reduced (by a factor of 6). This allows us to follow the life of crystallites from birth to impingement on each other. The time and spatial steps were $\Delta t = 1.31$ ns and $\Delta x = 13.1$ nm.

Results and Discussion

Anisotropic Solidification in 3D: Dendritic Solidification in $Al_{50.8}Ti_{49.2}$

We have performed simulations on a 480×480×480 grid to study polydendritic solidification in the $Al_{50.8}Ti_{49.2}$ alloy at $T = 1723$ K. Cubic crystalline symmetries and an interfacial free energy anisotropy of $\varepsilon_{3D} = 0.05$ have been assumed. The time evolution of the solidification morphology is shown in Figure 1. The solidification patterns we observe are consistent with previous results for single-crystal dendritic growth in 3D [6,22] and with our recent results for the Cu-Ni system [14]. Patterns evolving in 2D sections of the 3D simulation window (theoretical counterparts of classical metallographic images) are displayed in Figure 2 for the phase-, concentration-, and composition fields. The time evolution of the normalized transformed fraction X has been analyzed in terms of the Johnson-Mehl-Avrami-Kolmogorov kinetics [23], $X = 1 - \exp\{-(t/\tau)^p\}$, where τ is a constant related to the nucleation and growth rates, and p is the Avrami-Kolmogorov exponent characteristic to the mechanism of transformation. The kinetic exponent evaluated from our simulations is $p = 3.21 \pm 0.01$, falls between those for nucleation with diffusion controlled growth ($p = 2.5$) and with steady state growth ($p = 4$) [23]. This implies that some of the particles have not yet reached the fully grown steady state dendritic morphology, as apparent in Figures 1 and 2. Larger simulations are planned to clarify further the relation between morphology and p.

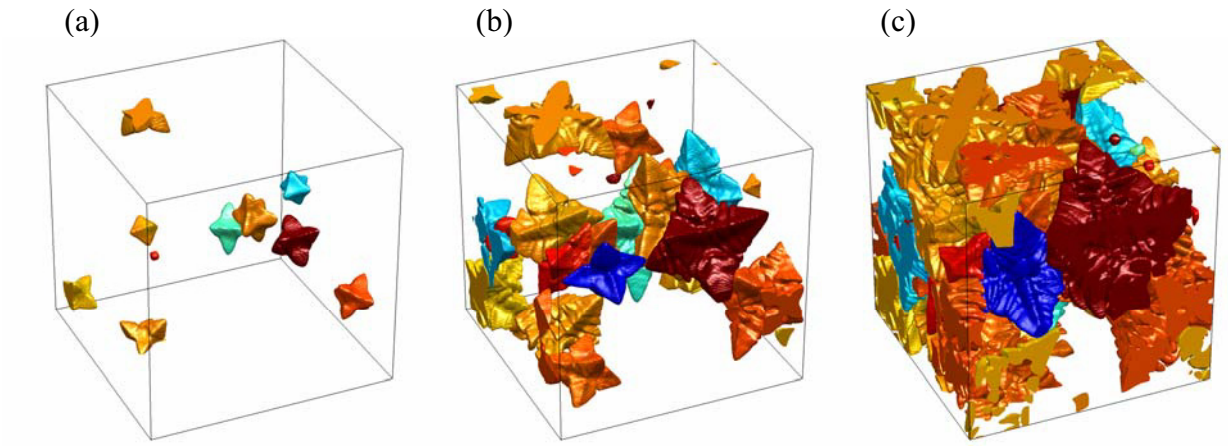

Figure 1. Snapshots showing the nucleation and growth of randomly oriented dendrites in the $Al_{50.8}Ti_{49.2}$ alloy (480×480×480 grid; interfacial free energy anisotropy of $\varepsilon_{3D} = 0.05$) at 4,000, 10,000 and 16,000 time steps. Note the effect of periodic boundary conditions: The branches that grow out of the simulation on one side of the simulation box enter on the opposite side.

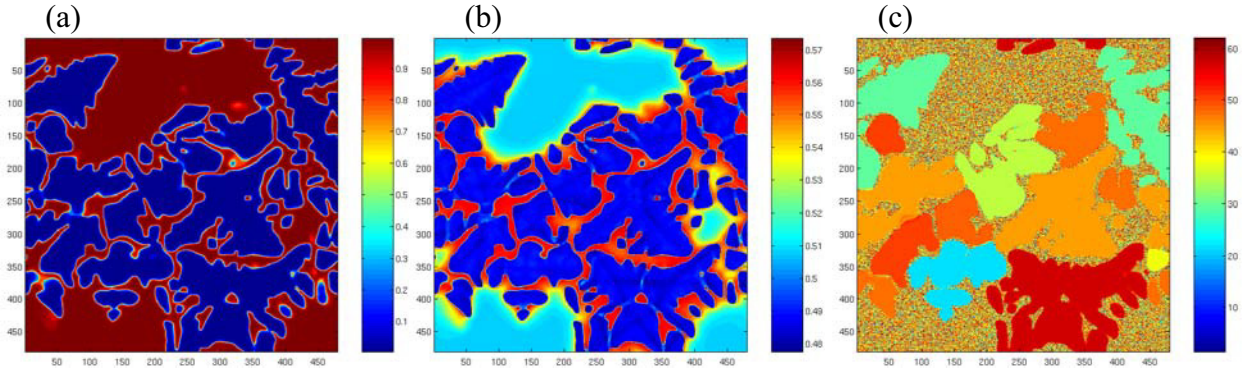

Figure 2. Cross-sectional (a) phase field, (b) concentration, and (c) orientation maps for the 265th horizontal layer of the snapshot shown in Figure 1(c). Note the random local orientation in the liquid, and the extended ordered layer ahead of the solidification front.

Morphology in Simulations with Confined Thickness

We have performed simulations to illustrate that our approach allows the modeling of solidification of thin films (Figure 3). Our preliminary results indicate that crystal morphology depends on the layer thickness. The relatively thick crystals resemble to the appropriate section of the "bulk" crystal, however, different morphologies are observed in thin layers (Figure 4). For example, in a thin layer, crystals nucleated with an orientation close to (111) show a remarkably isotropic (seaweed-like) geometry due to a smaller anisotropy for this section of the crystal than for others. Note that shapes displayed in Figure 4 cannot be grown in 2D simulations, which work with a single orientation field (such as those in [10-13]). Analysis of transformation kinetics yields $p = 2.37 \pm 0.01$, which is smaller than the $p \approx 3$ we found for steady state nucleation and growth in true 2D simulations for fully developed dendrites [11]. Larger simulations with better nucleation statistics are planned to reduce uncertainties due to small size. The observed difference in kinetic exponents may originate partly from the morphological variability of the 3D dendritic cross-sections, and the associated screening effects, which are known to reduce p via influencing particle impingement [24]. Another possibility, leading to a similar effect [11], is that for a significant fraction of the particles, steady state dendritic growth has not been yet established. Work is underway to clarify this issue.

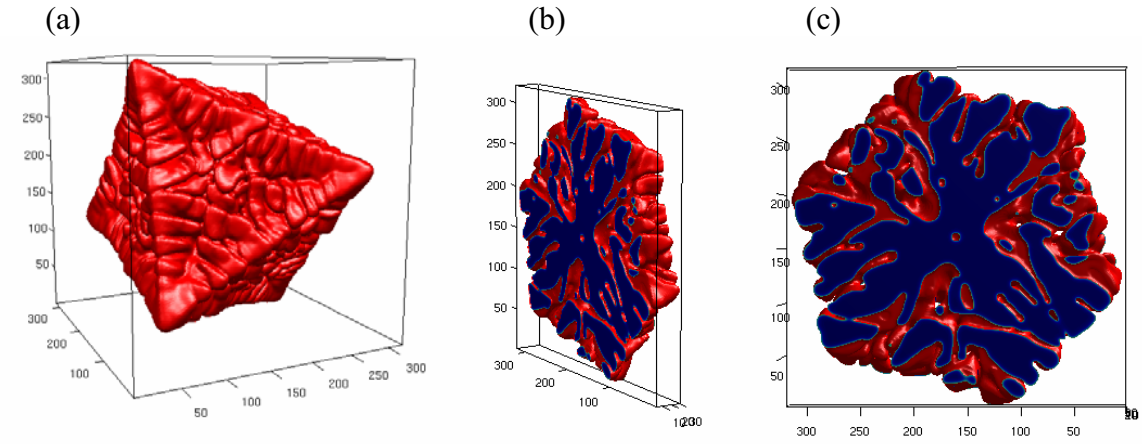

Figure 3. Morphologies grown at $S = 0.75$ in the Cu-Ni system with a kinetic anisotropy of $\varepsilon_{3D} = 0.2$. (a) Bulk single crystal grown on a 320×320×320 grid. (b) and (c): Two views of a crystal grown with its (111) direction parallel with the short axis. The latter simulation has been done on a 320×320×32 grid. The $\phi = 0.5$ surfaces are shown.

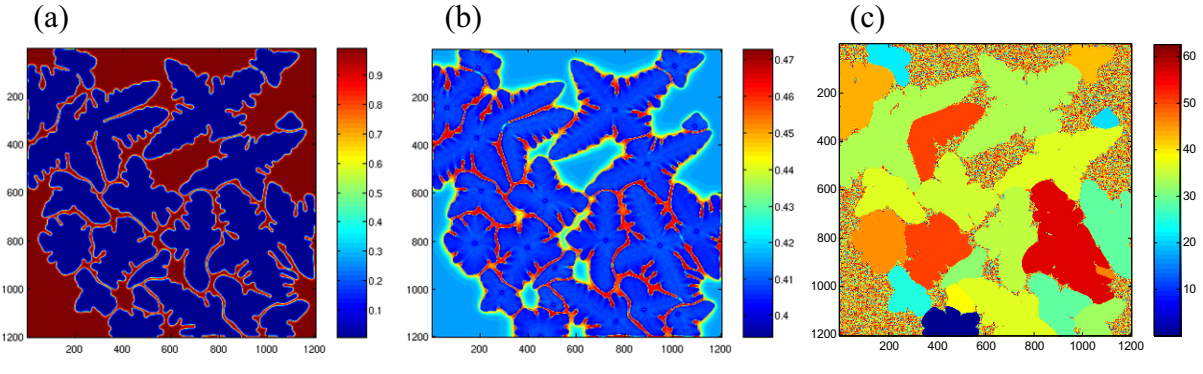

Figure 4. Polydendritic solidification in a very thin layer (1200×1200×2 grid) in the Cu-Ni system: Particles nucleated and grown with random orientation at $S = 0.75$, cubic crystal symmetries and a kinetic anisotropy of $\varepsilon_{3D} = 0.2$. Snapshots of the (a) phase field, (b) the concentration field, and (c) the crystallographic orientation are shown. In (c), the relative orientation with respect to the (111) direction is displayed.

Summary

We have investigated polycrystalline solidification in 3D in the framework of a phase field theory based on a quaternion representation of crystal orientation. Polydendritic solidification has been studied in the bulk and in thin films. Our simulations yield Avrami-Kolmogorov exponents of $p = 2.37 \pm 0.01$ and 3.21 ± 0.01 for crystallization in thin film and the bulk, respectively. The deviations from the values ($p = 3$ and 4) corresponding to a constant growth rate in 2 and 3D indicate that the simulated particles have not yet achieved steady state dendritic growth. Further work is needed to explore the effect of morphological transition between compact particles to fully developed dendrites on the kinetic exponent.

Acknowledgments

We thank A. Dinsdale (National Physical Laboratory, Teddington, UK) for providing thermodynamic data for Al-Ti-Nb. This work has been supported by contracts OTKA-T-037323 and ESA PECS No. 98005, and by the EU FP6 IP "IMPRESS" under Contract No. NMP3-CT-2004-500635, and forms part of the ESA MAP Projects No. AO-99-101 and AO-99-114. T.P. and G. B. acknowledge support by the Bolyai János Scholarship of the Hungarian Academy of Sciences.

References

1. R.W. Cahn, *The Coming of Materials Science* (Oxford, Pergamon, 2001).

2. V. Fleury, "Branched Fractal Patterns in Non-Equilibrium Electrochemical Deposition from Oscillatory Nucleation and Growth," *Nature*, 390 (6656) (1997), 145-148.

3. J.H. Magill, "Review Spherulites: A Personal Perspective," *J. Mater. Sci.*, 36 (13) (2001), 3143-3164.

4. K.L. Beers et al., "Combinatorial Measurement of Crystallization Growth Rate and Morphology in Thin Films of Isotactic Polystyrene," *Langmuir*, 19 (9) (2003), 3935-3940.

5. V. Ferreiro et al., "Growth Pulsations in Symmetric Dendritic Crystallization in Thin Polymer Blend Films," *Phys. Rev. E*, 65 (5) (2002), 051606-1-16.

6. J.J. Hoyt, M. Asta, and A. Karma, "Atomistic and Continuum Modeling of Dendritic Solidification," *Mater. Sci. Eng. R*, 41 (6) (2003), 121-163.

7. K. R. Elder et al., "Stochastic Eutectic Growth," *Phys Rev Lett*, 72 (5) (1994), 677-680.

8. I. Steinbach et al., "A Phase Field Concept for Multiphase Systems," *Physica D*, 94 (3) (1996), 135-147.

9. B. Nestler and A.A. Wheeler, " Phase-Field Modeling of Multi-Phase Solidification," *Comp Phys Comm*, 147 (1-2) (2002), 230-233.

10. R. Kobayashi, J.A. Warren, and W.C. Carter, "Vector-Valued Phase Field Model for Crystallization and Grain Boundary Formation," *Physica D*, 119 (3-4) (1998), 415-423.

11. L. Gránásy, T. Börzsönyi, and T. Pusztai, "Nucleation and Bulk Crystallization in Binary Phase Field Theory," *Phys Rev Lett*, 88 (20) (2002), 206105-1-4.

12. L. Gránásy et al., "Growth of 'Dizzy Denrites' ina a Random Field of Foreign Particles," *Nature Mater*, 2 (2) (2003), 92-96.

13. L. Gránásy et al., "A General Mechanism of Polycrystalline Growth," *Nature Mater*, 3 (9) (2004), 635-650.

14. T. Pusztai, G. Bortel, and L. Gránásy, "Phase Field Theory of Polycrystalline Solidification in Three Dimensions," *Europhys Lett*, 71 (1) (2005), 131-137.

15. R. Kobayashi and J.A. Warren, "Modeling the Formation and Dynamics of Polycrystals in 3D," *Physica A*, 356 (1) (2005), 127-132.

16. J.A. Warren and W.J. Boettinger, "Prediction of Dendritic Growth and Macrosegregation Patterns in a Binary Alloy Using the Phase-Field Method," *Acta Met Mater*, 43 (2) (1995), 689-703.

17. G.A. Korn and T.M. Korn, *Mathematical Handbook for Scientists and Engineers* (New York, McGraw-Hill, 1970) Chapter 14.10.

18. A. Karma and W.-J. Rappel, "Phase-Field Model of Dendritic Sidebranching with Thermal Noise," *Phys Rev E*, 60 (4) (1999), 3614-3625.

19. D.J. Jarvis and D. Voss, "IMPRESS Integrated Project - An Overwiev Paper," *Mater Sci Eng A*, 413-414 (2005), 583-591

20. A. Dinsdale (National Physical Laboratory, Teddington, UK), private communications during 2005. Binary limit of free energies for the Al-Ti-Nb system, based on Redlich-Kister polynomials.

21. J. Guo et al., "Phase-Field Simulation of Structure Evolution at High Growth Velocities During Directional Solidification of $Ti_{55}Al_{45}$ Alloy," *Intermetallics*, 13 (2005), 275-279.

22. J. Bragard et al., "Linking Phase-Field and Atomistic Simulations to Model DEndritic Solidification in Highly Undercooled Melts," *Interf Sci*, 10 (2-3) (2002), 121-136.

23. J.W. Christian, *The Theory of Transformations in Metals and Alloys* (Oxford: Pergamon, 1981).

24. T. Pusztai and L. Gránásy, "Mont Carlo Simulation of First-Order Phase Transformations with Mutual Blocking of Anisotropically growing Particles up to All Relevant Orders," *Phys Rev B*, 57 (22) (1998), 14110-14118.